International Journal of Biological Macromolecules 278 (2024) 134638

Contents lists available at ScienceDirect

International Journal of Biological Macromolecules

journal homepage: www.elsevier.com/locate/ijbiomac

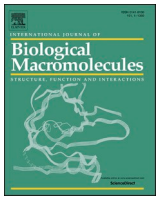

SARS-CoV-2 uses Spike glycoprotein to control the host's anaerobic metabolism by inhibiting LDHB

Vittoria Monaco [a,b], Ilaria Iacobucci [a,b], Luisa Canè [a,c], Irene Cipollone [a,b], Veronica Ferrucci [b,d], Pasqualino de Antonellis [b,d], Miriana Quaranta [e], Stefano Pascarella [e], Massimo Zollo [b,d], Maria Monti [a,b,*]

[a] Department of Chemical Sciences, University of Naples Federico II, 80126 Naples, Italy
[b] CEINGE Biotecnologie Avanzate "Franco Salvatore" S.c.a r.l., 80131 Naples, Italy
[c] Department of Translational Medical Sciences, University of Naples "Federico II", 80131 Naples, Italy
[d] Dipartimento di Medicina Molecolare e Biotecnologie Mediche (DMMBM), "Federico II" University of Naples, Naples 80131, Italy
[e] Sapienza Università di Roma, Department of Biochemical Sciences "A. Rossi Fanelli", Rome 00185, Italy

ARTICLE INFO

Keywords:
SARS-CoV-2
Spike glycoprotein
LDHB

ABSTRACT

The SARS-CoV-2 pandemic, responsible for approximately 7 million deaths worldwide, highlights the urgent need to understand the molecular mechanisms of the virus in order to prevent future outbreaks. The Spike glycoprotein of SARS-CoV-2, which is critical for viral entry through its interaction with ACE2 and other host cell receptors, has been a focus of this study. The present research goes beyond receptor recognition to explore Spike's influence on cellular metabolism. AP-MS interactome analysis revealed an interaction between the Spike S1 domain and lactate dehydrogenase B (LDHB), which was further confirmed by co-immunoprecipitation and immunofluorescence, indicating colocalisation in cells expressing the S1 domain. The study showed that Spike inhibits the catalytic activity of LDHB, leading to increased lactate levels in HEK-293T cells overexpressing the S1 subunit. In the hypothesised mechanism, Spike deprives LDHB of NAD^+, facilitating a metabolic switch from aerobic to anaerobic energy production during infection. The Spike-NAD^+ interacting region was characterised and mainly involves the W436 within the RDB domain. This novel hypothesis suggests that the Spike protein may play a broader role in altering host cell metabolism, thereby contributing to the pathophysiology of viral infection.

1. Introduction

Coronavirus disease 2019, commonly referred to as COVID-19, is caused by the Severe Acute Respiratory Syndrome Coronavirus 2 (SARS-CoV-2) which emerged in China in 2019 and then rapidly became a global pandemic. SARS-CoV-2 is a single-stranded RNA virus and its genome contains 14 open reading frames (ORFs) encoding for 29 viral proteins. These include 4 structural proteins, *i.e.* Spike (S), Membrane (M) and Envelope (E) glycoproteins and the Nucleocapsid (N) protein, 16 non-structural and 6 accessory proteins [1,2]. Once the cell is infected, the virus hijacks the host molecular machinery to promote its survival and proliferation [3]. In particular, one of the first common effects of cell infection by both DNA and RNA viruses is the metabolic reprogramming, including increased glycolysis, increased pentose phosphate activity to support nucleotide generation and, in general, the biosynthesis of all components required for the assembly of new virion particles, such as amino acids and lipids [3,4]. The close relationship between the metabolism and the SARS-CoV-2 replication has been well described and fits into this scenario [5–8]. Elevated serum glucose levels have been reported in COVID-19 patients, especially in the severe phenotypes [6]. In addition, patients with pre-existing metabolic disorders, including diabetes, have a higher risk of developing severe phenotypes [7]. A relevant feature of this altered metabolism, known as the 'Warburg Effect', is an increased glucose uptake and the abnormal fermentation of pyruvate to lactate [9,10]. The Warburg Effect is a hallmark of bacteria and viral infections, as well as of cancer [11]. Indeed, the activation of glycolysis has been reported in many oncogenic virus infections [4] such as Human Papilloma Virus (HPV), Hepatitis B Virus (HBV), Epstein-Barr Virus (EBV), Human T-Lymphotrophic Virus Type-1 (HTLV-1), and Merkel Cell Polyoma Virus (MCPyV) [12]. SARS-CoV-2

* Corresponding author at: Department of Chemical Sciences, University of Naples Federico II, 80126 Naples, Italy.
E-mail address: montimar@unina.it (M. Monti).

https://doi.org/10.1016/j.ijbiomac.2024.134638
Received 23 April 2024; Received in revised form 29 July 2024; Accepted 8 August 2024
Available online 13 August 2024

did not escape this reliance on the 'Warburg Effect', spreading rapidly in a hypoxic environment and sustaining glycolysis in infected lung endothelial cells [13]. Fermentative glycolysis, coupled with ATP production in the host cell, favours virus replication and the spread of the infection [9]. SARS-CoV-2, as well as other viruses, has been reported to interfere with mitochondrial metabolic functions to direct the host metabolism to meet its needs [14,15]. In fact, previous studies [16–18] on the influence of SARS-CoV-2 viral proteins on mitochondria and metabolic processes [2], highlighted the functional interaction of two viral proteins, Nps7 and Orf9c, with the respiratory electron transport process. In addition, the Membrane protein M was found to interact with proteins involved in mitochondrial metabolism [17].

The viral glycoprotein Spike (S), is mainly associated with the initial steps of infection, the viral entry process, through the recognition of specific receptors on the host cell surface [19]. Beyond its primary well-known role, several lines of evidence suggest that Spike may fulfil many other functions during the viral life cycle. Spike or its Receptor Binding Domain (RBD) has been reported to mediate the release of pro-inflammatory cytokines [20], influencers of leukocyte adhesion functions [21], endothelial cell barrier dysfunction and injury [22,23]. The relationship between Spike and/or its domains and the host metabolism has also been described in lung [24] and brain [25] endothelial cells, in which the impairment of several mitochondrial functions was observed. Analogous effects have also been reported in cardiomyocytes, where a short-term incubation (24 h) with Spike-S1 promoted ATP synthesis, whereas longer treatments led to mitochondrial damage through disruption of $\Delta\psi m$, mitochondrial Ca^{2+} overload and ROS accumulation [26].

In this paper, we investigated the role of the functional interaction between Spike from the alpha SARS-CoV-2 variant and LDHB, a protein partner that has been repeatedly identified in different cell lines, such as HEK-293T, Calu-3 and NCM460D, Caco-2, HK-2 [27]. The unbalance of lactate metabolism, including the alteration of lactate dehydrogenase (LDH) isozymes A and B, have been associated with worse outcomes in patients with SARS-CoV-2 infections [28,29]. By using *in vitro* and *ex vivo* biochemical approaches, we investigated the effects of the interaction between these two proteins on host energy metabolism and demonstrated an inhibitory effect of Spike protein on LDHB.

2. Results

2.1. Investigation of Spike interactome in HEK-293T and Calu-3

The study of the Spike glycoprotein interactome in HEK-293T and Calu-3 was performed using an affinity purification mass spectrometry-based approach (AP-MS). The full-length His-tagged Spike protein was employed as a bait to fish out its protein partners from protein extracts; the isolated proteins were then processed and identified by a shotgun approach. Briefly, purified intereractors were digested with trypsin, peptide mixtures were analysed by LC-MSMS and protein identification carried out with MaxQuant software; the proteins identified in the control (pre-cleaning step) were subtracted from those derived from AP. Moreover, the remaining proteins were also filtered using Crapome software, to further remove those identified as contaminants in approximately 50 % of the annotated experiments in the Crapome repository (Supplementary Table S1). Finally, we obtained 483 and 180 putative Spike interactors in HEK-293T and Calu-3, respectively.

The interactomes of Spike in HEK-293T and Calu-3 were then compared with the interactomes of Spike (S1 subunit) previously studied in similar experiments starting from three different cell lines [27], in

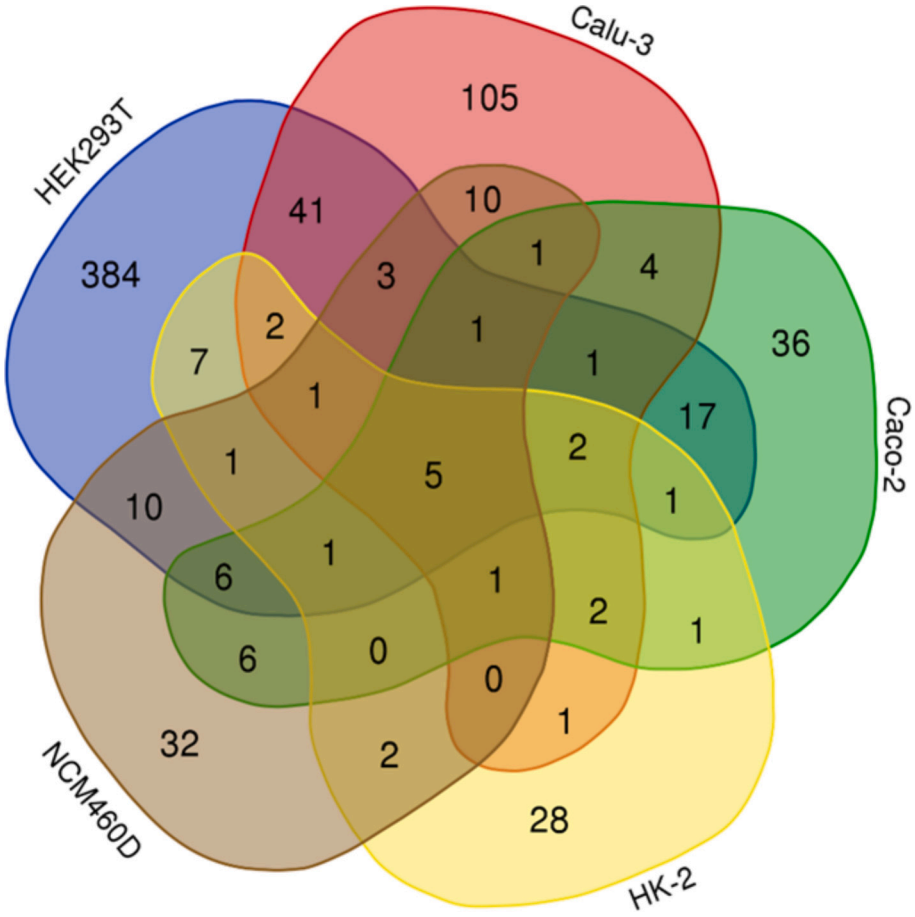

Fig. 1. Venn diagram representation of the comparison among Spike interactomes in HEK-293T, Calu-3, NCM460D, Caco-2, and HK-2 [27].

order to highlight and then investigate the functional interactions of Spike that are conserved regardless of the host cell type. The proteins shared among the five Spike interactomes are represented in the Venn diagram in Fig. 1.

By comparing the Spike's protein partners identified in HEK-293T and Calu-3 with the other interactomes, a total of 118 proteins, were in common at least within two interactomes, while 5 were shared across all conditions. These proteins were then functionally clustered using the ClueGO application of Cytoscape software (Fig. 2), with REACTOME as pathways database (FDR cut-off = 0.05).

The enriched terms related to metabolic processes, *i.e.* "Pyruvate metabolism and Citric Acid (TCA) cycle", "Glyoxylate metabolism and glycine degradation", "Pentose phosphate pathway" and "The citric acid (TCA) cycle and respiratory electron transport Citric Acid cycle (TCA cycle)" (FDRs, $8.9\ 10^{-10}$, $5.6\ 10^{-4}$, $3.7\ 10^{-4}$ and $7.2\ 10^{-6}$, respectively), caught our attention, as Spike has already been described to promote changes in mitochondrial metabolism, leading to a shift from aerobic to anaerobic metabolism [24].

These findings were also confirmed by a differential proteomics experiment, carried out to evaluate the effect of Spike-S1 on host cell proteome. In particular, the protein profile of HEK-293T cell line transfected with the S1 domain of the Spike protein was compared to the empty vector transfected cells (control) (see Supplementary Table S2). Among the proteins whose expression levels were significantly affected by the presence of Spike, we found some very relevant to glucose metabolism and/or the "Warburg Effect". In particular, hexokinase-2 (HK2), hypoxia up-regulated protein 1 (HYOU1) and TBC1 domain family member 4 (TBC1D4) were found to be up-regulated. HK2 is involved in the phosphorylation of glucose at the beginning of glycolysis. It is known that during viral infection, glucose uptake and degradation are greatly increased (Warburg Effect), leading to the accumulation of pyruvate, which is preferentially converted to lactate (anaerobic glycolysis) [11]. HYOU1 plays an important cytoprotective role under stressful conditions such as hypoxia. HYOU1 has been reported to promote glycolysis and malignant progression [30]. TBC1D4 promotes the insulin-induced translocation of the glucose transporter SLC2A4/GLUT4 at the plasma membrane, thereby increasing glucose uptake [31,32]. Among the down-regulated proteins, TBC1 domain family member 13 (TBC1D13) was notable. Indeed, TBC1D13 is a RabGAP and is a potent inhibitor of insulin-stimulated GLUT4 translocation [33]. Its down-regulation is in line with the promotion of glucose uptake, which typically occurs in the "Warburg Effect".

Since all our data point to a role for the Spike protein in the "Warburg Effect", we decided to further investigate the interaction between Spike and LDHB to elucidate the role of Spike in the switch from aerobic to anaerobic metabolism, possibly mediated by its (ubiquitous) interaction with this enzyme. Lactate Dehydrogenase B, LDHB, one of the five common interactors, is an isozyme of lactate dehydrogenase, which catalyses the oxidation of lactate to pyruvate through the concomitant reduction of the NAD^+ cofactor to NADH [34]; its role during viral infections, has been well described.

2.2. Investigation of Spike and LDHB interaction

The interaction between LDHB and Spike-S1 was validated by both co-immunoprecipitation (co-IP) and immunofluorescence (IF) experiments in HEK-293T cells overexpressing a FLAG-tagged construct of the SARS-CoV-2 Spike-S1 subunit belonging to the Wuhan reference sequence (alpha variant).

For the co-IP experiment, protein lysate was first pre-cleared on onto Protein G beads (control) and the unbound was then incubated with an anti-LDHB antibody immobilized on the same support. The pre-cleaning (PC) and IP eluates were analysed by Western blot by using anti-LDHB and anti-Spike S1 antibodies. As shown in Fig. 3A, the presence of a specific band at the expected molecular weight of the LDHB subunit in the IP lane confirmed the goodness of the experiment (lower panel). In addition, the presence of a band with an electrophoretic mobility coherent with S1 and detected by anti-Spike-S1 antibody in the IP lane confirmed the presence of the interaction between the two proteins (upper panel).

Immunofluorescence assays carried out in the same cell line (HEK-293T transiently transfected with FLAG- Spike-S1 protein) showed a high and widespread co-localization of this protein with LDHB (Fig. 3B third box, yellow dots). The co-localization between LDHB and Spike was also verified in Caco-2 cells infected with the Omega variant of SARS-CoV-2, as a model of the infection. In this system, LDHB and Spike also colocalise inside the cells (Fig. 3C third box, yellow dots). This last data confirmed that the co-localization between Spike and LDHB is ubiquitous and therefore conserved in different cellular systems. In addition, the IF data suggest that this interaction is preserved also in the presence of other Spike variants (*i.e.* Omega), although, the area of colocalization is roughly reduced compared to the Spike-S1 alpha

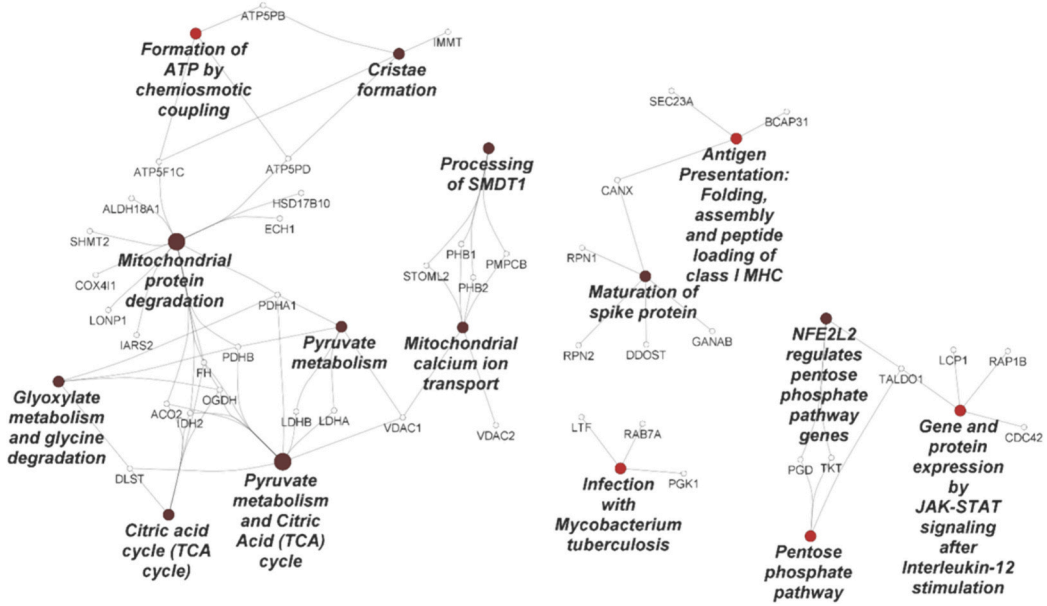

Fig. 2. Cytoscape functional enrichment analysis of the shared putative interactors among the 5 cell lines by using REACTOME database (FDR $\leq$ 0.05).

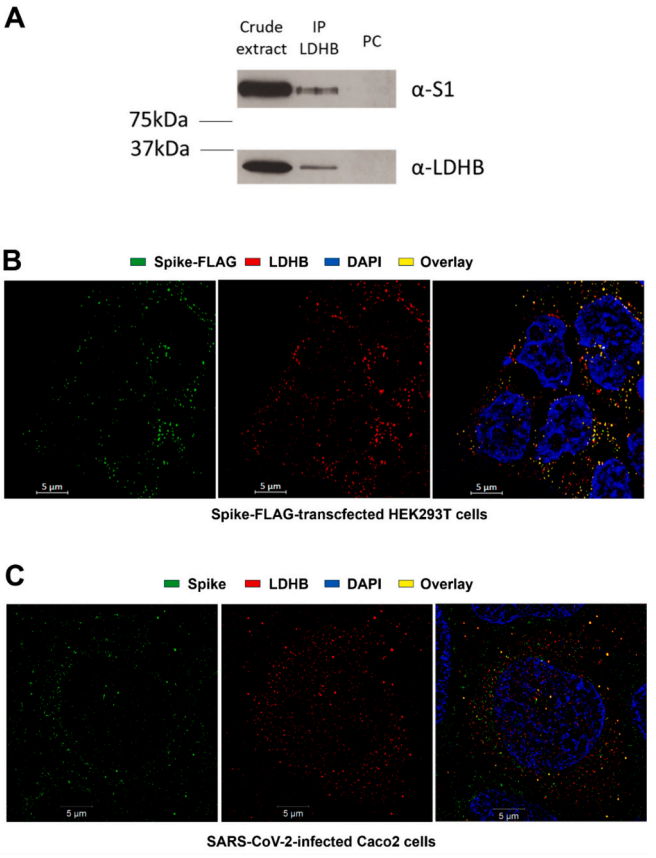

Fig. 3. (A) Co-immunoprecipitation experiment between LDHB and Spike S1-Flag proteins. (B) Immunofluorescence staining with antibodies against LDHB (red) and Spike S1-FLAG protein (green) on HEK-293T cells transiently transfected with plasmids expressing Spike S1-FLAG tag from SARS-CoV-2 (2019-nCoV; Wuhan). (C) Immunofluorescence staining with antibodies against LDHB (red) and Spike S1-FLAG protein (green) on Caco-2 cells infected with the Omega variant of SARS-CoV-2. DAPI was used for nuclear staining (blue). Scale bar, 5 μm.

variant.

In light of the above findings, we decided to elucidate the possible functional effect of the interaction between Spike and LDHB by performing an activity assay of LDHB in the presence of increasing concentrations of full-length recombinant Spike protein. In particular, we tested six concentrations of viral protein, ranging from 0 to 313 nM, with the LDHB concentration fixed at 500 nM. Enzyme activity was determined by monitoring the production of NADH in the subsequent LDHB-catalysed reaction:

$$L-\text{Lactic Acid} + NAD^+ \rightarrow \text{Pyruvate} + NADH.$$

The generation of NADH was coupled to the 1:1 reduction of a reporter dye to give a coloured (yellow) reaction product, the concentration of which was monitored by measuring the increase in absorbance at 450 nm. We observed a decreased activity of LDHB by increasing the concentration of full-length Spike protein, and the IC50 was also calculated (151.9 ± 22.10 nM) (Fig. 4A).

To confirm the intracellular inhibition of LDHB by Spike, lactate levels were measured in HEK-293T cells overexpressing Spike-S1, using a specific colourimetric assay (see Methods section). The data obtained were analysed using GraphPad software with a Mann-Whitney test between the two conditions (HEK-293T transfected with Spike-S1 or with the empty vector, control). The results reported in Fig. 4B, confirmed the occurrence of lactate accumulation in cells transfected with Spike-S1.

Having confirmed the interaction between LDHB and Spike-S1 also

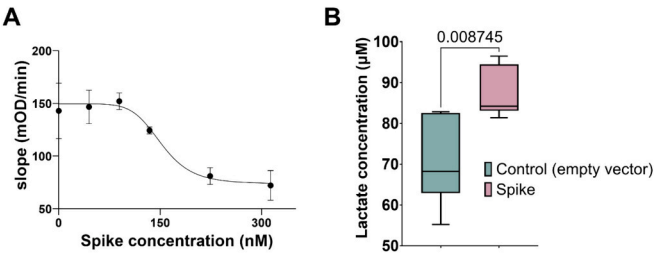

Fig. 4. (A) Activity assay plot of LDHB in the presence of full-length Spike. (B) Box and whisker plot of L-lactate concentration in HEK-293T cells transfected with SpikeS1-FLAG protein (pink box) and with empty vector (green box) (p value≤0.01).

in HEK-293T overexpressing the viral protein, we sought to investigate whether the interaction between the two proteins was direct. Pulldown experiments were performed with recombinant proteins (LDHB and tagged-S1 forms) both in the presence and in the absence of its cofactor NAD^+. Similarly, the interaction was also tested in the presence of LDHA isozyme; in each case, no interactions were highlighted (Supplementary Fig. S2, S3, and S4). These results suggest that the interaction between LDHB and Spike is not direct.

2.3. *Spike inhibits LDHB protein by subtracting NAD^+*

Given the absence of direct interaction between the two proteins, we postulated a possible mechanism for the inhibition process. We hypothesised that Spike may inhibit LDHB through the recruitment of its cofactor, NAD^+. To investigate this interaction, we used a limited proteolysis experiment coupled with mass spectrometry (LiP-MS) and docking simulations.

Limited proteolysis experiments coupled to mass spectrometry methodologies (LiP-MS) [35,36] were performed in parallel on the full-length Spike in the presence (molar ratio of 1:5) and in the absence of NAD^+. After incubation, all the samples were digested with proteinase K under limited proteolysis conditions (E:S ratio 1:100 for 1 min at 37 °C) and then extensively hydrolyzed using a standard shotgun trypsin-based protocol. Peptide mixtures were analysed by LC-MS/MS and the fold change for each peptide was calculated as the ratio of the mean of the peptide intensities among all replicates in the presence and in the absence of NAD^+. The putative binding sites were identified as the C-terminal amino acids of the down-regulated semi-tryptic peptides and, in the meantime, also present within the sequences of the up-regulated corresponding tryptic peptides [37]. Fig. 5A summarises the LiP-MS results; the peptides and their corresponding Fold Changes (FCs) are listed in Supplementary Table S3.

The cleavage sites identified on isolated protein and buried upon interaction with NAD^+ are shown on the three-dimensional structure of S1-Spike (Fig. 5A). In particular, the sites buried in the presence of NAD^+ and identified by LiP-MS fall within the region of the RBD (Receptor Binding Domain) motif from the residue 361 to 540 (see also the linear representation).

A computational analysis of the interaction between Spike and NAD^+ was also carried out by using docking simulation methods. The monomeric and fully trimeric Spike models (see Supplementary Materials) of the alpha variant were generated and different methods (CASTp, Fpocket, P2Rank) were used to predict the presence and position of potential binding pockets. Once the potentially involved regions were identified, docking was performed on both models, using two different approaches, AutoDock4 and AutoDock Vina. The results obtained provided a set of different poses for NAD^+ within a pocket located in the RBD region. In total, 38 possible conformations of NAD^+ within Spike were obtained: 19 from docking performed on the monomer and 19 on the trimer. No significant differences were found between the experiments carried out on the monomeric and the trimeric Spike. Comparing

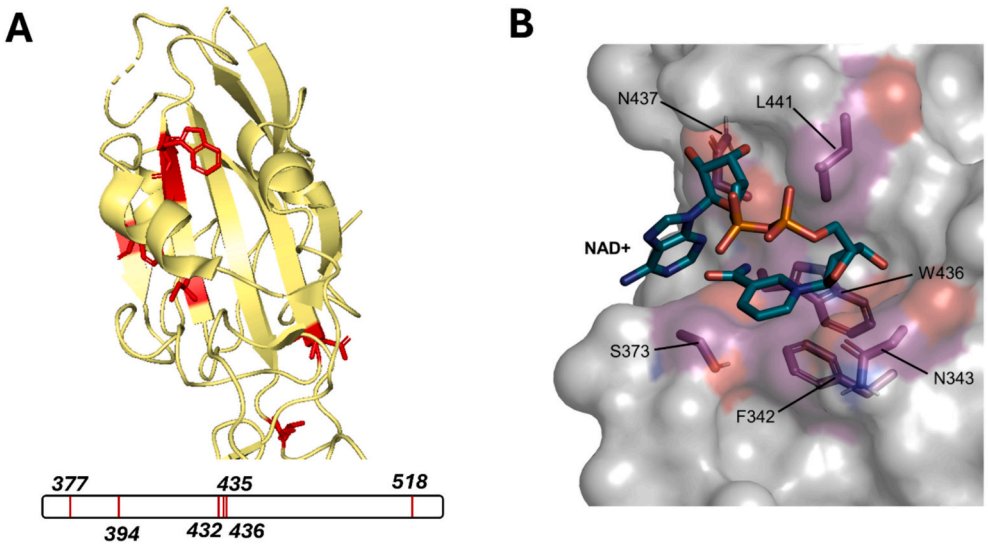

Fig. 5. (A) Three-dimensional representation of LiP-MS experiments for 361–540 region of the full-length Spike alpha glycoprotein. In red are the putative regions of interaction with NAD^+ (B) Predicted Spike-NAD^+ complex. The NAD^+ molecule and the interacting Spike residues are represented with labelled stick models. The Spike binding pocket is displayed with a transparent molecular surface.

all the results, it would still appear that NAD^+ tends to interact with residue W436 in many conformations, although not identically. Fig. 5B and S5 show the position of the binding pocket and the best mode of interaction between NAD^+ and Spike in terms of ligand-receptor interaction energy (−6.2 kcal/mol on an average of −5.88 kcal/mol) according to AutoDock Vina. Both LiP-MS data and docking simulation agree in localising the potential binding pocket of NAD^+ in the RBD region, and in identifying the W436 as one of the main mediators of this interaction. The critical role of W436 in the interaction with NAD^+ was further investigated by additional experiments on the W436V mutant of the Spike protein. First, a new docking analysis on a Spike protein model in which the W436 was replaced by a valine residue revealed a significant decrease in complex stability compared to the wt protein (−5.3 kcal/mol to an average of −4.9 kcal/mol) according to AutoDock Vina. Fig. 6A shows the rearrangement of the NAD^+ position within the previously identified binding pocket in the absence of the bulky side chain of tryptophan. In addition, we generated a HEK-293T cell line transiently transfected with a vector expressing the full-length mutant Spike W436V protein and assayed the catalytic activity of LDHB in both the protein extract expressing the wt and mutant Spike protein. As shown in Fig. 6B, an increase in the catalytic activity of LDHB was observed compared to the control (protein extract containing the wt Spike). This suggests that the substitution of W436 with valine leads to a reduction in the affinity between the Spike protein and NAD^+, with a consequent reduction in the inhibitory effect on LDHB.

3. Discussion

The SARS-CoV-2 Spike (S) glycoprotein is well documented to be associated with the viral recognition and entry processes. However, several recent studies carried out in different cell lines [38,39] have highlighted several unexpected roles beyond receptor recognition. Among others, Spike has been described to be involved in the release of pro-inflammatory mediators [20], in vesicle trafficking and the reprogramming of energy metabolism [24–26]. It is well established that several metabolic pathways, such as glycolysis, nutrient consumption and the "Warburg Effect" are generally enhanced during a viral infection. Despite the extensive literature describing the relationship between viral infection, hypoxia and the activation of anaerobic metabolism in different cell systems, this is the first time that a biochemical mechanism has been proposed to correlate the role of Spike with the aerobic-anaerobic metabolic switch, as confirmed by differential proteomics analysis. Furthermore, the central role of Spike in the energy metabolism of the host cell is supported by the identification of

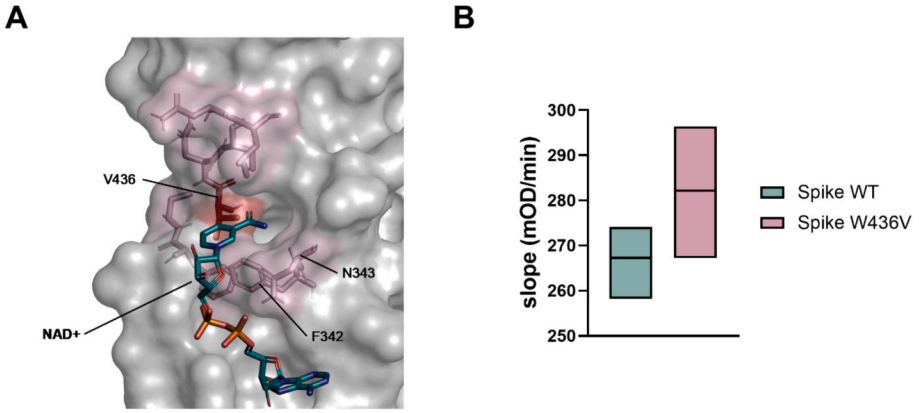

Fig. 6. (A) Binding site of the W436V Spike-NAD^+ complex. NAD^+ is shown as cyan sticks. Spike protein surface is shown in gray. Mutant Val436 is displayed as red sticks. Spike residues interacting with NAD^+ in all docking simulations are labelled and displayed as sticks. (B) Activity assay plot of LDHB in HEK-293T cells transiently transfected with plasmids expressing full-length Spike WT and W436V.

numerous interacting enzymes belonging to pyruvate metabolism and/or the tricarboxylic acid (TCA) cycle and/or glyoxylate metabolism and glycine degradation, such as FH, PDHB, PDHA1, IDH2, LDHB, LDHA, DLST, OGDH, ACO2, VDAC1.

Here, we investigate the role of Spike in influencing the host pyruvate metabolism through its interaction with LDHB. Lactate dehydrogenase (LDH) is an enzyme derived from the expression of four different genes: LDHA, LDHB, LDHC and LDHD. LDH has five isomeric forms, which are assembled into tetramers of either the more highly expressed subunits, the M (encoded by the LDHA gene) or the H (encoded by the LDHB gene). The composition of these tetramers varies according to tissue specificity.

LDHB has a higher affinity for lactate than LDHA [34], and its biological role is to oxidise lactate to pyruvate, by reducing its cofactor NAD^+ to NADH. Previous studies describe a correlation between the severity of SARS-CoV-2 infection and the increase in ROS, LDH and lactate in blood circulation [40,41]. Indeed, serum lactate is reported to be a metabolic marker of the severity level of COVID-19 disease [42]. It is now well-established that lactate serves as a mobile, energetic metabolite rather than a waste product; indeed, it has been found to be recycled and stored as glycogen in the liver, muscle, kidney, and brain (primarily astrocytes and not neurons) [43–46].

The accumulation of lactate within the cell can result from the inhibition of LDHB and/or the activation of LDHA. However, this balance is strongly dependent on the distribution of these isoenzymes in the tissues. Using an AP-MS approach, we repeatedly identified LDHB in all the interactomes analysed. The latter interaction was first validated intracellularly, by both immunoprecipitation (IP) and by immunofluorescence (IF) assays in HEK-293T cells transfected with a FLAG-tagged form of the Spike-S1 domain. The Spike-LDHB colocalization was further verified in a more physiopathological system consisting of Caco-2 cells infected with VOC OMICRON, EG.5, isolated from nasopharyngeal swabs of patient samples as previously described [47], suggesting that this functional interaction is critical for viral survival and spread and is therefore conserved among other viral variants. In addition, by treating HEK-293T-ACE2–infected cells with low concentration (5 μM) of gossypol, an inhibitor of LDH, an increase in the efficiency of viral infection/relication was detected, as evaluated by increased viral Nucleoprotein N [48]. This effect has been described also in other viral infections, confirming its importance for virus survival and proliferation. In Classical Swine Fever Virus (CSFV virus), LDHB was reported to be inhibited upon interaction with the viral protein NS3, and this inhibition promoted CSFV growth *via* mitophagy. Conversely, its overexpression impaired viral replication [49]. The role of LDHB is also reported by Kumar et al. in Polyomavirus-Positive (MCPyV+) and -Negative (MCPyV-) Merkel Cell Carcinoma (MCC). They demonstrated a tumour suppression effect by silencing LDHB in the MCPyV− MCC cell lines, suggesting a pro-oncogenic role for LDHB. However, they also show that in MCPyV+ MCC cell lines, silencing of the enzyme could promote cell growth. They correlate these different behaviours with evidence that the energy metabolism of virus-infected cells is strictly dependent on aerobic glycolysis [50]. The unbalance of lactate metabolism, which also results from the alteration of lactate dehydrogenase (LDH) isoenzymes A and B, have been associated with worse outcomes in patients with SARS-CoV-2 infection [28,29]. However, no hypothesis on the molecular process affecting LDHB activity has been proposed in any previously reported case.

For the first time, we demonstrated that LDHB is inhibited *in vitro* in the presence of Spike protein, with a dose-response trend. The latter data were corroborated by the accumulation of lactate in cells transfected with the S1 domain. This suggests a direct role for Spike in the "Warburg Effect" and that this role can be exerted by inhibiting LDHB.

However, this inhibition does not seem to derive from a direct interaction between the two proteins, as suggested by the negative results obtained in all pulldown experiments. These data are not unexpected, given that the experimental conditions in an AP-MS approach favour the stabilisation of whole multiprotein complexes rather than pairwise binding. Consequently, the observed interactions may result from both direct and indirect contacts between multiple proteins within the same multiprotein complex [51], a scenario consistent with the IF results showing intracellular co-localisation of LDHB and Spike. In view of these results and the inhibitory effect observed in the *in vitro* enzymatic assay, we speculated that the physical proximity between the two proteins might favour the subtraction of a part of the NAD^+ cofactor from LDHB by Spike, thus reducing the enzymatic efficiency of LDHB in the conversion of lactate to pyruvate. The NAD^+ cofactor is not covalently bound to the catalytic site of LDHB. LiP-MS experiments and docking simulations support this biochemical model, localising the potential NAD^+ binding site within the RBD of the S1 domain, in a three-dimensional pocket occurring from the residues 361 to 540 and mainly involving the W436. The position of the binding pocket and the importance of the W436 residue are also confirmed by the docking experiment carried out on the W436V Spike mutant. Indeed, the results show that NAD^+ tends to lose interaction with the residue at position 436 when it is replaced by a valine, with a binding energy higher than the original one, which suggests a lower affinity. This model was further validated by the increased activity of the LDHB enzyme observed in the presence of the full-length W436V Spike protein. Our findings not only confirm that the Spike protein has many important roles in addition to mediating viral entry, but for the first time, we propose a hypothesis for how it acts by directly influencing cellular metabolism, contributing to the molecular explanation of the "Warburg Effect" in SARS-CoV-2 infection.

4. Conclusion

The results of our studies could have a major impact on understanding one of the causes triggering the "Warburg effect", which is common in many other viral or bacterial infections. We believe that the proposed mechanism, involving subtraction of the NAD^+ cofactor from LDHB, could be a plausible inhibition mechanism in many infections, similar to that mediated by Spike in Covid-19. The interaction between Spike and NAD^+ as a mediator of the inhibitory effect on LDHB represents a new avenue for the development of therapies with peptide mimetics or drugs in general, capable of displacing/blocking this interaction, and thus favouring the restoration of the balance between aerobic and anaerobic metabolism.

5. Experimental

5.1. Cell cultures, transfection and infection

HEK-293T and Caco-2 cells (ATCC, Middlesex, UK; accession number: HTB-37L) were cultured in Dulbecco's modified Eagle's medium (DMEM; 41966–029; Gibco) supplemented with 10 % fetal bovine serum (FBS; 10270–106; Gibco), 2 mM L-glutamine (25030–024; Gibco), and 1 % penicillin/streptomycin (P0781; Sigma). HEK-293T cells (200.000 cells) were transiently transfected with the following plasmid DNA construct: SARS-CoV-2 (2019-nCoV) Spike S1 Gene ORF cDNA clone expression plasmid, C-FLAG tag (Cat: VG40591-*CF*. SinoBiological). Transient transfections were performed using the calcium phosphate method. Forty-eight hours after transfection, the HEK-293T cells were fixed for immunofluorescence analyses.

Caco2 cells (5 × 104) were plated on Glass Cover Slides Coverslips (18 mm Diameter Round Microscope) previously coated with type one collagen (PureCol® Type I Collagen Solution, 3 mg/mL, #5005, Advanced Biomatrix) for 30 min at room temperature. After 16 h, the cells were infected with SARS-CoV-2 viral particles belonging to VOC Omicron EG.5 (3 MOI) for a further 48 h, and then fixed in 4 % paraformaldehyde in PBS for 30 min for immunofluorescence (IF) analyses. SARS-CoV-2 (Variant Of Concern VOC OMICRON, EG.5) viruses were isolated from nasopharyngeal swabs of the patient's sample as

previously described [47]. These experiments were performed in an authorized BLS3 laboratory. For transient transfections of full-length Spike proteins, HEK293T (at ~70 % confluence) were briefly transfected with 5 μg DNA plasmid using X-tremeGENE 9 DNA Transfection Reagent (06365779001; Sigma-Aldrich) diluted with serum-free DMEM (41966–029; Gibco) to a concentration of 3 μL reagent/100 μL medium (3:1 ratio [μL]). Spike and Spike-Mut (W- > V) genes were synthesised and cloned into the pGen-lenti vector expression plasmid (GenScript Biotech - The Netherlands) and used for transfections. Transient transfections were performed according to the manufacturer's instructions. Briefly, X-tremeGENE 9 DNA transfection reagent was diluted with serum-free DMEM (41966-029; Gibco) (10 μL reagent/500 μL medium). Then, 5 μg of DNA plasmid was added to 500 μL of diluted X-tremeGENE 9 DNA Transfection Reagent. The transfection reagent: DNA complex was incubated for 15 min at room temperature and then added dropwise to the cells. Twelve hours after transfection, the cell culture medium was changed. At 48 h after the start of transfection, the cells were used for biochemical analyses. All experiments were performed in triplicate.

5.2. Affinity purification coupled with mass spectrometry (AP-MS) experiment

HEK-293T cells were lysed to obtain protein extracts, and the cell lines, were lysed as previously reported [27]. The Calu-3 cells were lysed as previously reported [52]. The SARS-CoV-2 Val16-Lys1211 Spike alfa recombinant protein with a C-terminal 6-His tag was purchased from R&D Systems (Minneapolis, Minnesota, Stati Uniti). A total of 2.5 μg of Spike was immobilized on 40 μL of slurry Dynabeads His tag (Thermo Fisher Scientific, Waltham, Massachusetts, United States), and incubated for 3 h at 4 °C. For the pre-clearing step, 4 mg of each membrane extract for HEK293T and 2 mg of total protein extract for Calu-3 were previously incubated with naked Dynabeads protein G (Thermo Fisher Scientific, Waltham, Massachusetts, United States) and Dynabeads His-tag (Thermo Fisher Scientific, Waltham, Massachusetts, United States) respectively, for 2 h at 4 °C to adsorb non-specific proteins. The HEK293T supernatants were first dialyzed with the buffer 50 mM Tris/HCl pH 8, 300 mM NaCl, 0.1 % Tween 20, and then incubated with the resin (Dynabeads His-tag) derivatized with the Spike protein overnight at 4 °C, whereas the Calu-3 supernatants were incubated directly with the functionalised support. The supernatants were removed, and the resin was washed with an extraction buffer. The proteins retained in the Spike pulldowns and on the pre- clearings resin were eluted with a buffer containing 5 % SDS. The pre-clearings eluates were used as controls. Proteins eluted from pulldowns and pre-clearings were digested with the S-Trap cartridges (Protifi, New York, United States) according to the manufacturer's protocol [53,54].

5.3. Bioinformatics analysis

The putative interactors of Spike protein were obtained from the list of proteins present in the pulldown experiment and absent in the control. Therefore, we removed the potential contaminants by using the Contaminant Repository for Affinity Purification (CRAPome) 2.0 web tool (https://reprint-apms.org) [55], by searching for the human experiment collection. All proteins found in at least 50 % of the experiments were tagged as contaminants. Pathway enrichment analysis was performed using the ClueGO 2.5.7 application of the Cytoscape software [56] by querying the Reactome database. Benjamini-Hochberg adjusted *p*-value (FDR) thresholds were set at 0.05.

5.4. Differential proteomics

HEK-293T cells, 48 h after transfection with SARS-CoV-2 Spike S1-FLAG, were lysed with 5 % sodium dodecyl sulfate (SDS, Biorad) and then sonicated with 3 pulses of 3 s for a total of 5 cycles. Protein extracts were centrifuged at 13000 rpm for 15 min, then the supernatants were filtered through compact column filters with lower filters with 90 μm pore size and finally quantified by PIERCE 660 nm assay (ThermoFisher). The equivalent of 30 μg of each protein extract was subjected to a shotgun proteomic approach, protein extracts were digested by trypsin on S-Trap filters [57], according to the manufacturer's protocol (Protifi, Huntington, NY).

5.5. Mass spectrometry

Peptide mixtures from the pulldown performed in the HEK293T cell lines were analysed using nanoAcquity UPLC (Waters) chromatographic system coupled with an LTQ Orbitrap XL mass spectrometer. Peptide mixtures were fractionated with a C18 capillary reverse-phase column (250 mm, 75 μm, 1.8 μm) working at a flow rate of 300 nL/min, using a non-linear 5–50 % gradient of eluent B (0.2 % formic acid, 95 % acetonitrile LC-MS Grade) over 260 min. Mass analyses were performed in Data Dependent Acquisition (DDA) mode by fragmenting the 10 most intense ions in the collision-induced dissociation (CID) modality. Peptide mixtures from the Calu-3 cell line pulldown and differential proteomics were analysed on an Orbitrap Exploris 240 instrument equipped with a Vanquish nanoLC system and Nanospray Flex ion source. Samples were fractionated on a C18 capillary reverse phase column (150 mm, 75 μm, 2 μm 100 Å) at a flow rate of 250 nL/min. A linear gradient of eluent B (0.2 % formic acid in 95 % acetonitrile) in A (0.2 % formic acid and 2 % acetonitrile in LC-MS grade water) was used from 2 % to 90 % in 45 min. The MS/MS method used a Data-Dependent Acquisition (DDA) mode consisting of a full scan from 375 to 1200 m/z range followed by fragmentation of the top 20 ions (MS/MS scan) selected by intensity and charge state (+2, +3 and multi-charges) with a dynamic exclusion time of 40 s. Protein identification was carried out by MaxQuant software (v.1.5.2.8), using the UniProt *Homo Sapiens* database as previously described (Palinski et al., 2021). The FDR cutoff was set up to 0.01 for each peptide and protein identification. The fixed modification was the carbamidomethyl (Cys), while the variable modifications were Gln- > pyro-Glu (N-term Gln) and Oxidation (Met). For differential proteomics, statistically significant proteins were evaluated using Perseus software. Statistical significance was determined by Student's *t*-test between samples and controls. Differences were considered statistically significant with a p-value <0.05 and a log2FC cut-off of 0.5.

5.6. Co-immunoprecipitation experiment

HEK-293T cells (200.000 cells), were lysed 48 h after transfection with SARS-CoV-2 Spike S1-FLAG, and 1 mg of protein extract was incubated with Dynabeads Protein G to perform a pre-clearing step for 2 h 30 min at 4 °C under agitation, used as control. The pre-clearing extract was then incubated with 2.5 μg of LDHB antibody for 16 h at 4 °C under agitation, and then incubated on Dynabeads Protein G support for the immunoprecipitation experiment for 3 h at 4 °C under agitation. The beads were then washed six times and eluted with a loading buffer. The eluates were then loaded onto an SDS-PAGE gel and transferred to a membrane to perform the Western Blot experiment. The membrane was cut and both sections were incubated with a blocking solution (PBS 1× and No-Fat Milk 5 %) for 1 h at room temperature. The membranes were then incubated with the appropriate primary antibodies overnight at 4 °C: anti-S1 (1:1000; GTX635708 Gene Tex), or anti-LDHB (1:1000, ab53292 Abcam), washed (PBS 1×, Tween 0.5 %) and incubated with the appropriate secondary antibodies (anti-Rabbit 1:10000 NA934V; anti-Mouse 1:5000 NA931V) for 45 min at room temperature. After washing the membrane was then incubated with an ECL solution (ThermoFisher Scientific) for 2 min and developed using a Chemidoc instrumentation (Biorad).

5.7. Immunofluorescence experiments

HEK-293T cells (200.000 cells), 48 h after transfection with SARS-

CoV-2 Spike S1-FLAG and/or SARS-CoV-2-infected Caco2 cells were fixed in 4 % paraformaldehyde in PBS for 30 min, washed three times with PBS, and permeabilised for 15 min with 0.1 % Triton X-100 (215680010; Acros Organics) diluted in PBS. HEK-293T cells were then washed with PBS and blocked with Antibody Diluent Block (ARD1001EA, Perkin Elmer) for 1 h at room temperature (RT). The samples were incubated overnight at 4 °C with the appropriate primary antibodies: anti-Flag (1:200; F1804, Sigma), or anti-LDHB (1:200, ab53292 Abcam). After washing twice with PBS, the samples were incubated for 1 h at room temperature with the appropriate secondary antibody: anti-mouse Alexa Fluor 647 (1:200; ab150115; Abcam) or anti-rabbit Alexa Fluor 546 (1:200, A10040, Invitrogen). The SARS-CoV-2-infected Caco2 cells were washed with PBS and blocked with 3 % BSA (A9418; Sigma) in PBS for 1 h at room temperature. The samples were incubated overnight at 4 °C with the appropriate primary antibodies: anti-Spike (1:150; GTX6357D8), or anti-LDHB (as above). After washing twice with PBS, the samples were incubated with the appropriate secondary antibody for 1 h at room temperature: anti-rabbit Alexa Fluor 546 (1:200; #A10040, Thermo Fisher Scientific) or anti-mouse Alexa Fluor 488 (1:200, ab150113, Abcam). DNA was stained with DAPI (1:1000; #62254; ThermoFisher). The slides were washed and mounted with cover sLiPs with 50 % glycerol (G5150; Sigma-Aldrich). Microscopy images were obtained with the Elyra 7 platform (Zeiss) with the optical Lattice SIM2 technology and processed with the ZEN software (Zeiss, black edition), using the 63× oil immersion objective.

5.8. LDHB activity assay

An activity assay kit (ab140361 Abcam) was used to test the activity of the LDHB recombinant protein in the presence and absence of different concentrations of Spike recombinant glycoprotein. All reagents and samples were prepared as suggested by the specific manufacturing protocol. Briefly, 100 μL of a solution of LDHB 500 nM or 500 μg/mL for the protein extracts were prepared in 1× Incubation buffer of the kit and added to each wells and only the 1× Incubation buffer was employed as zero standards. The wells were covered and incubated for 2 h at room temperature in constant agitation of 70 rpm. At the end of the incubation period, the unbound supernatants were removed from each well and then washed three times with 300 μL of 1× Wash Buffer. For the activity in the presence of the recombinant proteins, after complete removal of the last wash, the zero controls and samples were incubated with 50 μL of different concentrations of Spike recombinant protein, as reported in the table, for 30 min at room temperature in constant agitation of 70 rpm. Finally, were have been added in each well 50 μL or 100 μL of freshly prepared 2× or 1× Activity Solution (1× NAD^+, 1× Coupler and 1× Reagent Dye), for the LDHB recombinant protein or the protein extracts, respectively. The absorbances were read in a kinetic experiment as follows: kinetic mode, 450 nm as wavelength, 30 min with 12-s intervals, using the Benchmark Plus (BioRad) instrumentation. For all the samples recorded the slopes were then used for the processing analysis. The analysis was performed by using GraphPad software v.9.5.1. The concentration of Spike protein and the slopes were processed with a nonlinear 4-parameters fitting test.

5.9. L-lactate assay

For the L-lactate assay, a kit (ab65331 Abcam) was used as recommended by the manufacturer, 2×10^6 HEK-293T cells transfected with SARS-CoV-2 (2019-nCoV) Spike S1 and with an empty vector (as control) were resuspended in 4× volumes of Lactate Assay Buffer (200 μL), rapidly homogenized, and centrifuged for 5 min at 13000 rpm at 4 °C. The supernatants were subjected to a PCA/KOH deproteinization step. Perchloric acid (PCA) was added with a final concentration of 1 M, homogenized, and incubated on ice for 5 min. Samples were then centrifuged at 13,000 rpm for 2 min at 4 °C. Excess of PCA was precipitated by adding a final percentage of 34 % of ice-cold 2 M KOH, the pH was checked to be in the range 6.5–8 the samples were centrifuged at 13,000 rpm for 15 min at 4 °C. The supernatants and a 1:1 dilution of these with Lactate Assay buffer (50 μL) were used for the assay and loaded in duplicate in a 96-well plate with a calibration curve. All the samples and standards were incubated for 30 min at room temperature protected from the light with the recommended reaction mix. Internal controls, as suggested by the assay kit manufacturer, were also prepared as the background sample controls by using the same samples incubated with a reaction mix depleted of the enzyme mix. Measurement was carried out in an absorbance modality on an EnSpire multimode plate reader (PerkinElmer) instrumentation at 450 nm. Sample absorbances were normalized to the background of the blank and control samples, then interpolated using the calibration curve e multiplied by the dilution factor, and finally, the concentrations were adjusted as a percentage of the original concentration (calculated as the ratio of the initial and the final volumes after the deproteinization step, as suggested by the manufacturer). The concentration values of the diluted (1:1) and not-diluted samples were plotted in GraphPad software v.9.5.1 to perform a Mann-Whitney test with a 1 % FDR cut-off.

5.10. Limited proteolysis coupled with mass spectrometry (LiP-MS)

The Spike glycoproteins alone were used as a control and the complex formation was obtained by incubating of the protein-ligand system in a molar ratio of 1:5 for 30 min in a thermomixer at room temperature with stirring in a PBS 1× solution at pH 7.4. Limited proteolysis was performed with the enzyme proteinase K at a weight ratio of 1:100 for 1 min at 37 °C with stirring. The reaction was stopped at a temperature of 95 °C for 5 min. All samples and controls were incubated with dithiothreitol (DTT) 12 mM in PBS 1× pH 7.4 for 30 min at 37 °C followed by iodoacetamide (IAM) 40 mM in PBS 1× pH 7.4 in the dark for 30 min. The reaction was stopped by rapid desalting using a ZipTip C18 system. The resulting mixtures were dried using a SpeedVac system and then processed by extensive hydrolysis, by using trypsin at a weight ratio of 1:50 at 37 °C overnight and then stopped by the addition of 20 % TFA in a volume ratio of 1:10. Samples were dried using a SpeedVac system. The peptide mixtures were resuspended in 16 μL of 0.2 % formic acid (HCOOH) LC-MS grade, and 4 μL of these were injected and analysed by the mass spectrometer in technical duplicate. The instrument used was an LTQ-Orbitrap XL (ThermoFisher Scientific) mass spectrometer equipped with a nano-ESI ion source (ThermoFisher Scientific) and nanoAcquity UPLC system (Waters). Peptide fractionation was performed on a reverse-phase C18 capillary column (250 mm, 75 μm, 1.8 μm) working at a flow rate of 300 nL/min from 5 % to 50 % of eluent B (0.2 % formic acid, 95 % acetonitrile) in 35 min. Mass analyses were performed in Data Dependent Acquisition (DDA) mode by fragmenting the 5 most intense ions in the Collision-Induced Dissociation (CID) mode. Experiments were performed in triplicate. Protein identification and quantification were performed with MaxQuant software (v.1.5) using the raw files and the specific FASTA database of the Spike glycoprotein. Identification and quantification were performed with an FDR cut-off of 0.01 and using carbamidomethyl (Cys) as the fixed modification, while Gln- > pyro-Glu (N-term Gln) and oxidation (Met) were used as the variable modifications. The MaxQuant output table "peptides" was used for the identification of the putative binding sites. All identified peptides were filtered and peptides with >1 zero in the replicates were removed, then the following selective criteria were used: tryptic peptides with Fold Change >1.5, semi-tryptic peptides with Fold Change <0.5, all tryptic and semi-tryptic peptide pairs complementary to each other. Fold changes were calculated as the ratio of the average LFQ Intensity of the peptide in the complex divided by average LFQ Intensity of the peptide in the protein alone. Protein visualization was performed using PyMOL software. The binding residues obtained from the LiP-MS experiment are highlighted in red.

5.11. Molecular docking

The three-dimensional model of the Spike B.1.1.7 variant structure was generated using the MODELLER 10.4 software [58], using the Spike structure 6VXX from the PDB database as a template. The characteristic mutations of the B.1.1.7 (Alpha) variant of SARS-CoV-2 were taken from the outbreak.info database [59]. The structural model of the W436V Spike mutant was obtained by performing site-specific mutagenesis using PyMOL (The PyMOL Molecular Graphics System, Version 2.0 Schrodinger, LLC) on the previously generated structure. Prediction of Spike potential binding sites was performed using specialised methods: CASTp 3.0 (http://sts.bioe.uic.edu/castp), Fpocket (https://fpocket.sourceforge.net/), and P2Rank (https://prankweb.cz/) [60–62]. The interaction between Spike and NAD^+ was investigated by *in-silico* docking. The three-dimensional structure of the NAD^+ molecule was downloaded from the PubChem database (PubChem ID 5892) in Structured Data File (SDF) format. The SDF of the molecule was converted to PDB format using the molecular graphics software PyMOL. *In silico* docking was performed using the AutoDock4 [63] and AutoDock Vina [64,65] software using the monomer and trimer structures of the Spike protein. The results of the binding site predictions were used to select the position of the grids: the grid maps were positioned by circumscribing the region containing the most recurrent amino acid residues predicted to be part of a binding site, and consistent with the LiP-MS experiment. Docking was performed with a grid box of 82 × 92 × 100 points and a grid point spacing of 0.375 Å for AutoDock4 and with a grid box of 30 × 28 × 38 points and a grid point spacing of 1 Å for AutoDock Vina. The docking experiment conducted on the W436V Spike mutant was performed with AutoDock Vina under the same conditions as described above. The complexes calculated from the docking procedures were displayed in PyMOL, to compare the conformations of NAD^+ in different poses. The Spike-NAD^+ interactions were analysed using LIGPLOT [66].

Supplementary data to this article can be found online at https://doi.org/10.1016/j.ijbiomac.2024.134638.

Funding

This research was funded by the project 'CEINGE-TASK-FORCE-2022 COVID19', POR Campania FESR 2014/2020, CUP: D63C22000570002 and 'CEINGE TaskForce COVID19', code D64I200003800 by Regione Campania for the fight against COVID-19, DGR no. 140; 17 March 2020.

CRediT authorship contribution statement

Vittoria Monaco: Writing – original draft, Methodology, Investigation, Formal analysis, Conceptualization. **Ilaria Iacobucci:** Methodology, Investigation. **Luisa Canè:** Visualization, Investigation. **Irene Cipollone:** Visualization, Investigation. **Veronica Ferrucci:** Visualization, Investigation. **Pasqualino de Antonellis:** Visualization, Investigation. **Miriana Quaranta:** Visualization, Investigation. **Stefano Pascarella:** Writing – original draft, Resources. **Massimo Zollo:** Writing – original draft, Supervision, Resources, Funding acquisition. **Maria Monti:** Writing – review & editing, Writing – original draft, Supervision, Resources, Project administration, Conceptualization.

Declaration of competing interest

The authors declare that they have no known competing financial interests or personal relationships that could have appeared to influence the work reported in this paper.

Acknowledgements

We thank the President of CEINGE, Prof. Pietro Forestieri and the CEO of CEINGE, Dr. Mariano Giustino for the collaborative support of the program, within the Regione Campania Covid19 Taskforce and the BSL3 facility at CEINGE. We further thank the work performed by Dr. Marco Miceli (CEINGE Biotecnologie Avanzate "Franco Salvatore") for handling virus experiments as presented into the manuscript. We also thank the Sapienza University of Rome, to have supported the research of Stefano Pascarella with the grant RP122181671E8B2F.

References

[1] A.L. Tornesello, et al., Immune profiling of SARS-CoV-2 epitopes in asymptomatic and symptomatic pediatric and adult patients, J. Transl. Med. 21 (1) (Feb. 2023) 123, https://doi.org/10.1186/s12967-023-03963-5.
[2] S. Justo Arevalo, et al., What do we know about the function of SARS-CoV-2 proteins? Front. Immunol. 14 (2023) 1249607 https://doi.org/10.3389/fimmu.2023.1249607.
[3] K. Yang, et al., Cardiovascular dysfunction in COVID-19: association between endothelial cell injury and lactate, Front. Immunol. 13 (2022) 868679, https://doi.org/10.3389/fimmu.2022.868679.
[4] S.K. Thaker, J. Ch'ng, H.R. Christofk, Viral hijacking of cellular metabolism, BMC Biol. 17 (1) (Jul. 2019) 59, https://doi.org/10.1186/s12915-019-0678-9.
[5] P. Chen, M. Wu, Y. He, B. Jiang, M.-L. He, Metabolic alterations upon SARS-CoV-2 infection and potential therapeutic targets against coronavirus infection, Signal Transduct. Target. Ther. 8 (1) (Jun. 2023) 237, https://doi.org/10.1038/s41392-023-01510-8.
[6] B. Shen, et al., Proteomic and metabolomic characterization of COVID-19 patient sera, Cell 182 (1) (Jul. 2020) 59–72.e15, https://doi.org/10.1016/j.cell.2020.05.032.
[7] F.F. Costa, W.R. Rosário, A.C. Ribeiro Farias, R.G. de Souza, R.S. Duarte Gondim, W.A. Barroso, Metabolic syndrome and COVID-19: an update on the associated comorbidities and proposed therapies, Diabetes Metab. Syndr. 14 (5) (2020) 809–814, https://doi.org/10.1016/j.dsx.2020.06.016.
[8] S. Ajaz, et al., Mitochondrial metabolic manipulation by SARS-CoV-2 in peripheral blood mononuclear cells of patients with COVID-19, Am. J. Phys. Cell Phys. 320 (1) (Jan. 2021) C57–C65, https://doi.org/10.1152/ajpcell.00426.2020.
[9] J. Pouysségur, I. Marchiq, S.K. Parks, J. Durivault, M. Ždralević, M. Vucetic, "Warburg effect" controls tumor growth, bacterial, viral infections and immunity - genetic deconstruction and therapeutic perspectives, Semin. Cancer Biol. 86 (Pt 2) (Nov. 2022) 334–346, https://doi.org/10.1016/j.semcancer.2022.07.004.
[10] M.V. Liberti, J.W. Locasale, The Warburg effect: how does it benefit Cancer cells? Trends Biochem. Sci. 41 (3) (Mar. 2016) 211–218, https://doi.org/10.1016/j.tibs.2015.12.001.
[11] I. Barba, L. Carrillo-Bosch, J. Seoane, Targeting the Warburg effect in Cancer: where do we stand? Int. J. Mol. Sci. 25 (6) (Mar. 2024) 3142, https://doi.org/10.3390/ijms25063142.
[12] C. Berrios, et al., Merkel cell polyomavirus small T antigen promotes pro-glycolytic metabolic perturbations required for transformation, PLoS Pathog. 12 (11) (Nov. 2016) e1006020, https://doi.org/10.1371/journal.ppat.1006020.
[13] P. Icard, et al., The key role of Warburg effect in SARS-CoV-2 replication and associated inflammatory response, Biochimie 180 (Jan. 2021) 169–177, https://doi.org/10.1016/j.biochi.2020.11.010.
[14] A. Cavezzi, E. Troiani, S. Corrao, COVID-19: hemoglobin, iron, and hypoxia beyond inflammation. A narrative review, Clin Pract 10 (2) (May 2020) 1271, https://doi.org/10.4081/cp.2020.1271.
[15] J. Saleh, C. Peyssonnaux, K.K. Singh, M. Edeas, Mitochondria and microbiota dysfunction in COVID-19 pathogenesis, Mitochondrion 54 (Sep. 2020) 1–7, https://doi.org/10.1016/j.mito.2020.06.008.
[16] J. Li, et al., Virus-host Interactome and proteomic survey reveal potential virulence factors influencing SARS-CoV-2 pathogenesis, Med 2 (1) (Jan. 2021), https://doi.org/10.1016/j.medj.2020.07.002, pp. 99-112.e7.
[17] D.E. Gordon, et al., A SARS-CoV-2 protein interaction map reveals targets for drug repurposing, Nature 583 (7816) (Jul. 2020) 459–468, https://doi.org/10.1038/s41586-020-2286-9.
[18] D.E. Gordon, et al., Comparative host-coronavirus protein interaction networks reveal pan-viral disease mechanisms, Science 370 (6521) (Dec. 2020), https://doi.org/10.1126/science.abe9403 p. eabe9403.
[19] E. Behboudi, et al., SARS-CoV-2 mechanisms of cell tropism in various organs considering host factors, Heliyon 10 (4) (Feb. 2024) e26577, https://doi.org/10.1016/j.heliyon.2024.e26577.
[20] R.-G. Zhang, X.-J. Liu, Y.-L. Guo, C.-L. Chen, SARS-CoV-2 spike protein receptor binding domain promotes IL-6 and IL-8 release via ATP/P2Y2 and ERK1/2 signaling pathways in human bronchial epithelia, Mol. Immunol. 167 (Mar. 2024) 53–61, https://doi.org/10.1016/j.molimm.2024.02.005.
[21] J.P. Robles, M. Zamora, E. Adan-Castro, L. Siqueiros-Marquez, G. Martinez de la Escalera, C. Clapp, The spike protein of SARS-CoV-2 induces endothelial inflammation through integrin α5β1 and NF-κB signaling, J. Biol. Chem. 298 (3) (Mar. 2022), https://doi.org/10.1016/j.jbc.2022.101695, p. 101695.
[22] B. Bhargavan, G.D. Kanmogne, SARS-CoV-2 spike proteins and cell-cell communication induce P-selectin and markers of endothelial injury, NETosis, and inflammation in human lung microvascular endothelial cells and neutrophils: implications for the pathogenesis of COVID-19 coagulopathy, Int. J. Mol. Sci. 24 (16) (Aug. 2023), https://doi.org/10.3390/ijms241612585, p. 12585.

[23] S.B. Biering, et al., SARS-CoV-2 spike triggers barrier dysfunction and vascular leak via integrins and TGF-β signaling, Nat. Commun. 13 (1) (Dec. 2022) 7630, https://doi.org/10.1038/s41467-022-34910-5.
[24] K. Zekri-Nechar, et al., Spike protein subunits of SARS-CoV-2 Alter mitochondrial metabolism in human pulmonary microvascular endothelial cells: involvement of factor Xa, Dis. Markers 2022 (2022) 1118195, https://doi.org/10.1155/2022/1118195.
[25] E.S. Kim, M.-T. Jeon, K.-S. Kim, S. Lee, S. Kim, D.-G. Kim, Spike proteins of SARS-CoV-2 induce pathological changes in molecular delivery and metabolic function in the brain endothelial cells, Viruses 13 (10) (Oct. 2021) 2021, https://doi.org/10.3390/v13102021.
[26] T.V. Huynh, L. Rethi, T.-W. Lee, S. Higa, Y.-H. Kao, Y.-J. Chen, Spike protein impairs mitochondrial function in human cardiomyocytes: mechanisms underlying cardiac injury in COVID-19, Cells 12 (6) (Mar. 2023) 877, https://doi.org/10.3390/cells12060877.
[27] I. Iacobucci, et al., Spike S1 domain interactome in non-pulmonary systems: a role beyond the receptor recognition, Front. Mol. Biosci. 9 (2022) 975570, https://doi.org/10.3389/fmolb.2022.975570.
[28] A.G. Vassiliou, et al., Lactate kinetics reflect organ dysfunction and are associated with adverse outcomes in intensive care unit patients with COVID-19 pneumonia: preliminary results from a GREEK single-centre study, Metabolites 10 (10) (Sep. 2020) 386, https://doi.org/10.3390/metabo10100386.
[29] T.P. Velavan, L.T. Kieu Linh, A. Kreidenweiss, J. Gabor, S. Krishna, P.G. Kremsner, Longitudinal monitoring of lactate in hospitalized and ambulatory COVID-19 patients, Am. J. Trop. Med. Hyg. 104 (3) (Jan. 2021) 1041–1044, https://doi.org/10.4269/ajtmh.20-1282.
[30] J.-M. Wang, J.-Y. Jiang, D.-L. Zhang, X. Du, T. Wu, Z.-X. Du, HYOU1 facilitates proliferation, invasion and glycolysis of papillary thyroid cancer via stabilizing LDHB mRNA, J. Cell. Mol. Med. 25 (10) (May 2021) 4814–4825, https://doi.org/10.1111/jcmm.16453.
[31] C.P. Mîinea, et al., AS160, the Akt substrate regulating GLUT4 translocation, has a functional Rab GTPase-activating protein domain, Biochem. J. 391 (1) (Oct. 2005) 87–93, https://doi.org/10.1042/BJ20050887.
[32] D. Baus, et al., Identification of a novel AS160 splice variant that regulates GLUT4 translocation and glucose-uptake in rat muscle cells, Cell. Signal. 20 (12) (Dec. 2008) 2237–2246, https://doi.org/10.1016/j.cellsig.2008.08.010.
[33] J.R. Davey, et al., TBC1D13 is a RAB35 specific GAP that plays an important role in GLUT4 trafficking in adipocytes, Traffic 13 (10) (Oct. 2012) 1429–1441, https://doi.org/10.1111/j.1600-0854.2012.01397.x.
[34] C.J. Valvona, H.L. Fillmore, P.B. Nunn, G.J. Pilkington, The regulation and function of lactate dehydrogenase a: therapeutic potential in brain tumor, Brain Pathol. 26 (1) (Jan. 2016) 3–17, https://doi.org/10.1111/bpa.12299.
[35] S. Schopper, et al., Measuring protein structural changes on a proteome-wide scale using limited proteolysis-coupled mass spectrometry, Nat. Protoc. 12 (11) (Nov. 2017) 2391–2410, https://doi.org/10.1038/nprot.2017.100.
[36] D. Raineri, et al., Osteopontin binds ICOSL promoting tumor metastasis, Commun Biol 3 (1) (Oct. 2020) 615, https://doi.org/10.1038/s42003-020-01333-1.
[37] A. Holfeld, J.-P. Quast, R. Bruderer, L. Reiter, N. de Souza, P. Picotti, Limited proteolysis-mass spectrometry to identify metabolite-protein interactions, Methods Mol. Biol. 2554 (2023) 69–89, https://doi.org/10.1007/978-1-0716-2624-5_6.
[38] C. Bamberger, S. Pankow, S. Martínez-Bartolomé, J.K. Diedrich, R.S.K. Park, J. R. Yates, Analysis of the tropism of SARS-CoV-2 based on the host Interactome of the spike protein, J. Proteome Res. 22 (12) (Dec. 2023) 3742–3753, https://doi.org/10.1021/acs.jproteome.3c00387.
[39] F. Saadi, D. Pal, J.D. Sarma, Spike glycoprotein is central to coronavirus pathogenesis-parallel between m-CoV and SARS-CoV-2, Ann. Neurosci. 28 (3–4) (Jul. 2021) 201–218, https://doi.org/10.1177/09727531211023755.
[40] B.M. Henry, et al., Lactate dehydrogenase levels predict coronavirus disease 2019 (COVID-19) severity and mortality: a pooled analysis, Am. J. Emerg. Med. 38 (9) (Sep. 2020) 1722–1726, https://doi.org/10.1016/j.ajem.2020.05.073.
[41] A. Cavezzi, R. Menicagli, E. Troiani, S. Corrao, COVID-19, cation dysmetabolism, sialic acid, CD147, ACE2, viroporins, hepcidin and ferroptosis: a possible unifying hypothesis, F1000Res 11 (2022) 102, https://doi.org/10.12688/f1000research.108667.2.
[42] G.S. Gupta, The lactate and the lactate dehydrogenase in inflammatory diseases and major risk factors in COVID-19 patients, Inflammation 45 (6) (Dec. 2022) 2091–2123, https://doi.org/10.1007/s10753-022-01680-7.
[43] G.A. Brooks, Cell-cell and intracellular lactate shuttles, J. Physiol. 587 (Pt 23) (Dec. 2009) 5591–5600, https://doi.org/10.1113/jphysiol.2009.178350.
[44] G.A. Brooks, The science and translation of lactate shuttle theory, Cell Metab. 27 (4) (Apr. 2018) 757–785, https://doi.org/10.1016/j.cmet.2018.03.008.
[45] C. Calì, A. Tauffenberger, P. Magistretti, The strategic location of glycogen and lactate: from body energy reserve to brain plasticity, Front. Cell. Neurosci. 13 (2019) 82, https://doi.org/10.3389/fncel.2019.00082.
[46] P. Sonveaux, et al., Targeting lactate-fueled respiration selectively kills hypoxic tumor cells in mice, J. Clin. Invest. 118 (12) (Dec. 2008) 3930–3942, https://doi.org/10.1172/JCI36843.
[47] V. Ferrucci, et al., Long-chain polyphosphates impair SARS-CoV-2 infection and replication, Sci. Signal. 14 (690) (Jul. 2021) eabe5040, https://doi.org/10.1126/scisignal.abe5040.
[48] P. de Antonellis, et al., Targeting ATP2B1 impairs PI3K/Akt/FOXO signaling and reduces SARS-COV-2 infection and replication, EMBO Rep. 25 (7) (Jul. 2024) 2974–3007, https://doi.org/10.1038/s44319-024-00164-z.
[49] S. Fan, et al., LDHB inhibition induces mitophagy and facilitates the progression of CSFV infection, Autophagy 17 (9) (Sep. 2021) 2305–2324, https://doi.org/10.1080/15548627.2020.1823123.
[50] S. Kumar, et al., MiR-375 regulation of LDHB plays distinct roles in polyomavirus-positive and -negative Merkel cell carcinoma, Cancers (Basel) 10 (11) (Nov. 2018) 443, https://doi.org/10.3390/cancers10110443.
[51] I. Iacobucci, V. Monaco, F. Cozzolino, M. Monti, From classical to new generation approaches: an excursus of -omics methods for investigation of protein-protein interaction networks, J. Proteome 230 (Jan. 2021) 103990, https://doi.org/10.1016/j.jprot.2020.103990.
[52] M. Di Sanzo, et al., Ferritin heavy chain binds peroxiredoxin 6 and inhibits cell proliferation and migration, Int. J. Mol. Sci. 23 (21) (Oct. 2022) 12987, https://doi.org/10.3390/ijms232112987.
[53] I. Andolfo, et al., Proteome alterations in erythrocytes with PIEZO1 gain-of-function mutations, Blood Adv. 7 (12) (Jun. 2023) 2681–2693, https://doi.org/10.1182/bloodadvances.2022008673.
[54] F. Cozzolino, et al., New label-free methods for protein relative quantification applied to the investigation of an animal model of Huntington disease, PLoS One 15 (9) (2020) e0238037, https://doi.org/10.1371/journal.pone.0238037.
[55] D. Mellacheruvu, et al., The CRAPome: a contaminant repository for affinity purification–mass spectrometry data, Nat. Methods 10 (8) (Aug. 2013) 730–736, https://doi.org/10.1038/nmeth.2557.
[56] G. Bindea, et al., ClueGO: a Cytoscape plug-in to decipher functionally grouped gene ontology and pathway annotation networks, Bioinformatics 25 (8) (Apr. 2009) 1091–1093, https://doi.org/10.1093/bioinformatics/btp101.
[57] W. Palinski, et al., Lysosome purinergic receptor P2X4 regulates neoangiogenesis induced by microvesicles from sarcoma patients, Cell Death Dis. 12 (9) (Aug. 2021) 797, https://doi.org/10.1038/s41419-021-04069-w.
[58] A. Sali, T.L. Blundell, Comparative protein modelling by satisfaction of spatial restraints, J. Mol. Biol. 234 (3) (Dec. 1993) 779–815, https://doi.org/10.1006/jmbi.1993.1626.
[59] K. Gangavarapu, et al., Outbreak.info genomic reports: scalable and dynamic surveillance of SARS-CoV-2 variants and mutations, Nat. Methods 20 (4) (Apr. 2023) 512–522, https://doi.org/10.1038/s41592-023-01769-3.
[60] W. Tian, C. Chen, X. Lei, J. Zhao, J. Liang, CASTp 3.0: computed atlas of surface topography of proteins, Nucleic Acids Res. 46 (W1) (Jul. 2018) W363–W367, https://doi.org/10.1093/nar/gky473.
[61] V. Le Guilloux, P. Schmidtke, P. Tuffery, Fpocket: an open source platform for ligand pocket detection, BMC Bioinformatics 10 (1) (Dec. 2009) 168, https://doi.org/10.1186/1471-2105-10-168.
[62] L. Jendele, R. Krivak, P. Skoda, M. Novotny, D. Hoksza, PrankWeb: a web server for ligand binding site prediction and visualization, Nucleic Acids Res. 47 (W1) (Jul. 2019) W345–W349, https://doi.org/10.1093/nar/gkz424.
[63] G.M. Morris, et al., AutoDock4 and AutoDockTools4: automated docking with selective receptor flexibility, J. Comput. Chem. 30 (16) (Dec. 2009) 2785–2791, https://doi.org/10.1002/jcc.21256.
[64] J. Eberhardt, D. Santos-Martins, A.F. Tillack, S. Forli, AutoDock Vina 1.2.0: new docking methods, expanded force field, and Python bindings, J. Chem. Inf. Model. 61 (8) (Aug. 2021) 3891–3898, https://doi.org/10.1021/acs.jcim.1c00203.
[65] O. Trott, A.J. Olson, AutoDock Vina: improving the speed and accuracy of docking with a new scoring function, efficient optimization, and multithreading, J. Comput. Chem. 31 (2) (Jan. 2010) 455–461, https://doi.org/10.1002/jcc.21334.
[66] A.C. Wallace, R.A. Laskowski, J.M. Thornton, LIGPLOT: a program to generate schematic diagrams of protein-ligand interactions, Protein Eng. Des. Sel. 8 (2) (1995) 127–134, https://doi.org/10.1093/protein/8.2.127.